Cardiac muscle patches containing four types of cardiac cells derived from human pluripotent stem cells improve recovery from cardiac injury in mice

Xi Lou ¹, Yawen Tang¹, Lei Ye¹, Danielle Pretorius¹, Vladimir G. Fast¹, Asher M. Kahn-Krell¹, Jue Zhang², Jianhua Zhang^{3,4}, Aijun Qiao¹, Gangjian Qin¹, Timothy Kamp^{3,4}, James A. Thomson^{2,4}, and Jianyi Zhang^{1,5}*

¹Department of Biomedical Engineering, School of Medicine and School of Engineering, University of Alabama at Birmingham, 1670 University Boulevard, Volker Hall G094J, Birmingham, AL 35294, USA; ²Morgridge Institute for Research, Madison, WI 53715, USA; ³Division of Cardiovascular Medicine, Department of Medicine, University of Wisconsin-Madison, WI, USA; ⁴Department of Cell and Regenerative Biology, University of Wisconsin-Madison, Madison, WI, USA; and ⁵Department of Medicine, School of Medicine, University of Alabama at Birmingham, Birmingham, AL 35294, USA

Received 11 June 2022; revised 24 October 2022; accepted 4 November 2022; online publish-ahead-of-print 17 January 2023

Aims

of Cardiology

We have shown that human cardiac muscle patches (hCMPs) containing three different types of cardiac cells—cardiomyocytes (CMs), smooth muscle cells (SMCs), and endothelial cells (ECs), all of which were differentiated from human pluripotent stem cells (hPSCs)—significantly improved cardiac function, infarct size, and hypertrophy in a pig model of myocardial infarction (MI). However, hPSC-derived CMs (hPSC-CMs) are phenotypically immature, which may lead to arrhythmogenic concerns; thus, since hPSC-derived cardiac fibroblasts (hPSC-CFs) appear to enhance the maturity of hPSC-CMs, we compared hCMPs containing hPSC-CMs, -ECs, and -CFs (4TCC-hCMPs) with a second hCMP construct that lacked hPSC-CFs but was otherwise identical [hCMP containing hPSC-CMs, -AECs, and -SMCs (3TCC-hCMPs)].

Methods and results

hCMPs were generated in a fibrin scaffold. MI was induced in severe combined immunodeficiency (SCID) mice through permanent coronary artery (left anterior descending) ligation, followed by treatment with cardiac muscle patches. Animal groups included: MI heart treated with 3TCC-hCMP; with 4TCC-hCMP; MI heart treated with no patch (MI group) and sham group. Cardiac function was evaluated using echocardiography, and cell engraftment rate and infarct size were evaluated histologically at 4 weeks after patch transplantation. The results from experiments in cultured hCMPs demonstrate that the inclusion of cardiac fibroblast in 4TCC-hCMPs had (i) better organized sarcomeres; (ii) abundant structural, metabolic, and ion-channel markers of CM maturation; and (iii) greater conduction velocities (31 \pm 3.23 cm/s, P < 0.005) and action-potential durations (APD50 = 365 ms \pm 2.649, P < 0.0001; APD = 408 ms \pm 2.757, P < 0.0001) than those (velocity and APD time) in 3TCC-hCMPs. Furthermore, 4TCC-hCMPs transplantation resulted in better cardiac function [ejection fraction (EF) = 49.18% \pm 0.86, P < 0.05], reduced infarct size (22.72% \pm 0.98, P < 0.05), and better engraftment (15.99% \pm 1.56, P < 0.05) when compared with 3TCC-hCMPs (EF = 41.55 \pm 0.92%, infarct size = 39.23 \pm 4.28%, and engraftment = 8.56 \pm 1.79%, respectively).

Conclusion

Collectively, these observations suggest that the inclusion of hPSC-CFs during hCMP manufacture promotes hPSC-CM maturation and increases the potency of implanted hCMPs for improving cardiac recovery in mice model of MI.

^{*} Corresponding author. Tel: +(205) 934 8421; fax: +(205) 934 9101, E-mail: jayzhang@uab.edu

[©] The Author(s) 2023. Published by Oxford University Press on behalf of the European Society of Cardiology.

Graphical Abstract

Cardiac Fibroblasts Promote Cardiomyocyte Maturation in Engineered Cardiac Muscle Patch and Improve Functional Recovery In Hearts with AMI hPSCs hPSC-CMs hPSC-AECs hPSC-CFs hPSC-SMCs Multi-component patch Rocker 1 Angiogenesis 1 Remodeling 1 Scar formation murine MI model

Keywords

Heart failure • Human pluripotent stem cell • Tissue engineering • Myocardial infarction

1. Introduction

Patients with severe acute myocardial infarction (MI) often progress to end-stage congestive heart failure (CHF), which is one of the most significant problems in public health. From a cellular perspective, heart failure is caused by the loss of the contractile unit of the left ventricle (LV): cardiomyocytes (CMs). Currently, heart transplantation surgery remains the only available treatment for end-stage CHF, and the supply of donated hearts is far lower than the number of patients in need of treatment. Thus, the fundamental goal of regenerative myocardial therapy is to repopulate the scarred region of an infarcted heart with functioning CMs, and promising results have been reported in preclinical studies conducted with transplanted cells or engineered cardiac tissues. ^{1–10} However, the effectiveness of these approaches is limited by a number of obstacles, including maturation of CMs, poor engraftment, and integration of the implanted cells/tissues within the native myocardium.

Like human embryonic stem cells (hESCs), human-induced pluripotent stem cells (hiPSCs) have an unlimited capacity for self-replication and can differentiate into cells of any other tissue of important organs. ¹¹ Protocols using human pluripotent stem cells (hPSCs), which refer to both hESCs¹² and hiPSC, ¹³ to differentiate into the four primary cardiaccell types (CMs), smooth muscle cells (SMCs), endothelial cells (ECs),

and cardiac fibroblasts (CFs), have been well established. 1-4 The mixed ma- 9. trix with hiPSC-CMs, -SMCs, and -ECs, as well as human cardiac muscle patches (hCMPs) constructed from all three cell types: hiPSC-CMs, -SMC, and -ECs (3TCC-hCMPs), have been associated with significant improvements in cardiac function and infarct size when administered to infarcted pig hearts. 7,14 However, hPSC-derived cardiomyocytes 5 (hPSC-CMs) are phenotypically more similar to foetal or neonatal CMs than to the CMs of adult hearts, and this immaturity may lead to arrhythmogenic concerns. 15,16 hPSC-derived cardiac fibroblasts (hPSC-CFs) enhance the maturation of hPSC-CMs, ¹⁷ and the roles of CFs during heart = development and in maintaining myocardial architecture and connectivity $\stackrel{\sim}{\bowtie}$ under both normal physiological conditions and in response to injury are becoming increasingly apparent. ¹⁸ Thus, we hypothesize that the inclusion of hPSC-CFs during hCMP manufacture will promote hPSC-CM maturation and increase the potency of hCMPs for myocardial repair. The current report tests this hypothesis by conducting experiments both in vitro and in a murine MI model with hCMPs containing hPSC-CMs, -SMCs, -ECs, and -CFs (4TCC-hCMPs) and a second hCMP construct that lacks hPSC-CFs but is otherwise identical (3TCC-hCMPs). Notably, experiments were also conducted with hPSC-derived arterial ECs (hPSC-AECs) rather than conventional hPSC-ECs, because some evidence suggests that hPSC-AECs more effectively support arteriogenesis. 19,20

2. Methods

hESCs and hiPSCs were expanded and subcultured as previously described. 14,21 Briefly, cells were thawed, seeded onto Corning® 6-well plates that had been coated with Matrigel®, expanded in mTESR medium (STEMCELL Technologies), and incubated in a humidified atmosphere with 5% CO2 at 37°C until 80–90% confluent.

2.1 Generation of cardiac cells from hPSCs

hPSC-CMs were differentiated from hiPSCs reprogrammed from human CF with the CytoTune^TM-iPS Reprogramming Kit (Invitrogen) as previously reported. 14,21,22 Briefly, 1×10^6 hiPSCs were expanded on a Matrigel-coated dish for 4 days; then, differentiation was induced by culturing the cells in RPMI 1640 medium supplemented with 2% B27 minus insulin (RPMI/B27-; Thermo Fisher Scientific) and 12 μ M CHIR99021 (a glycogen synthase kinase 3 β inhibitor; Tocris) for 24 h, in RPMI/B27- medium for 48 h, and then with the Wnt inhibitor IWR-1 for 48 h. Beating cells usually appeared about 8 days after differentiation was initiated, and the hPSC-CMs were purified by culturing them for 4–7 days in glucose- and pyruvate-free RPMI1640 medium (Invitrogen) supplemented with 4 mM lactate.

hPSC-derived SMCs (hPSC-SMCs) were differentiated from hiPSCs reprogrammed from human CF with the CytoTuneTM-iPS Reprogramming Kit (Invitrogen) as previously reported. Briefly, hiPSCs were treated with CHIR99021 and ascorbic acid for 5 days to induce mesoderm differentiation; then, hiPSCs with a vascular progenitor cell phenotype (hiPSC-VPCs) were collected via magnetic nanoparticle selection for CD34 expression (EasySepTM Human CD34 Positive Selection Kit II; STEMCELL Technologies). SMC differentiation was induced by culturing the hiPSC-VPCs on collagen IV-coated dishes with SmGM-2 medium (Lonza, USA) containing platelet-derived growth factor BB (PDGF-BB) and transforming growth factor $\beta1$ (TGF $\beta1$). After differentiation, the hPSC-SMCs were cultured with 4 mM lactate RPMI1640 metabolic medium for 4–6 days for selective enrichment.

To generate hPSC-AECs, a puromycin resistance cassette was inserted into the promoter-regulatory region of the PECAM1 allele of H9 hESCs [WA09, National Institutes of Health (NIH) registry number 0062] and the cells were differentiated as described previously. 19 Briefly, hESCs were differentiated into mesoderm cells from Day 0 to Day 2 with E8BAC media [E8 media supplemented with 5 ng/mL bone morphogenic protein 4 (BMP4), 25 ng/mL Activin-A, and 1 µM CHIR99021]; then, the cells were cultured from Day 2 to Day 6 in E5 media [Dulbecco's Modified Eagle Medium (DMEM)/F12 with L-ascorbic acid-2-phosphate magnesium, sodium selenium, NaHCO₃, transferrin] supplemented with 100 ng/mL fibroblast growth factor (FGF), 50 ng/mL vascular endothelial growth factor (VEGF), 10 μM SB431542, 5 μM RESV (Sigma-Aldrich, USA), and 10 µM L690. Puromycin (2.5 µg/mL) was added to the media from Day 4-6 to eliminate non-ECs, and hPSC-AECs were maintained in FVIR medium (E5 with 20 µg/mL insulin, 100 ng/mL of FGF, 50 ng/mL of VEGF, 10 µM SB431542, and 5 µM RESV) on vitronectin-coated dishes; puromycin was added for another 2 days during the maintenance period.

For differentiation into hPSC-CFs, DF19-9-11 T hiPSCs (WiCell Institute) were expanded until 100% confluent⁴; then, the medium was changed to RPMI/B27⁻ supplemented with 12 μ M CHIR99021 (Tocris) for 24 h, to RPMI/B27⁻ for 24 h, and to cardiac fibroblast differentiation basal (CFB) medium (DMEM, high glucose with HAS, linoleic acid, lecithin, ascorbic acid, GlutaMAX, hydrocortisone hemisuccinate, rh insulin) supplemented with 75 ng/mL bFGF (WiCell Research Institute) for 18 days; the CFB/bFGF medium was changed every other day.

2.2 Flow cytometry analyses

Cells were trypsinized, resuspended as single cells, fixed in 4% paraformal-dehyde (PFA), permeabilized in 0.1% Triton X-100 at 4°C for 10 min, blocked with 0.5% bovine serum albumin (BSA) in phosphate-buffered saline (PBS) without $\text{Ca}^{2+}/\text{Mg}^{2+}$ at room temperature for 7 min, and incubated with the indicated primary antibodies, isotype-control antibodies, and secondary antibodies; then, the cells were washed, resuspended in

2% foetal calf serum (FCS)/PBS containing 5 μL of propidium iodide (10 $\mu g/mL),$ and evaluated with a FACS Aria instrument (BD Biosciences, USA) and FlowJo software.

2.3 Surface marker expression

The hPSC-derived cardiac cells were characterized via immunostaining as described previously. 7,14,23 Briefly, the cells were fixed with 4% PFA for 20 min at room temperature, permeabilized in 0.2% Triton X-100 at 4°C for 15 min, and then blocked with 5% donkey serum in PBS, pH 7.4, for 30 min. hPSC-CMs were incubated with mouse anti- α -sarcomeric actin (αSA , Sigma-Aldrich, USA), mouse or rabbit anti-cardiac troponin T (cTnT, Abcam, USA), and rabbit anti-cadherin (CDH2, Abcam, USA) primary antibodies; hPSC-AECs were incubated with goat anti-CD31 (Santa Cruz Biotech, USA), rabbit anti-vascular endothelial (VE)-cadherin (Abcam, USA), and rabbit anti-von Willebrand factor (VWF, Abcam, USA) primary antibodies; hPSC-SMCs were incubated with mouse anti-α-smooth muscle actin (α-SMA, Sigma-Aldrich, USA), goat antismooth muscle 22 alpha (SM22, Santa Cruz Biotech, USA), and rabbit anti-calponin 1 (Santa Cruz Biotech, USA) primary antibodies; and hPSC-CFs were incubated with mouse anti-clone TE-7 fibroblast (TE-7. Sigma-Aldrich, USA), rabbit anti-vimentin (Abcam, USA), mouse anti-α-SMA (Sigma-Aldrich, USA), and rabbit anti-calponin 1 primary antibodies; then, the primary antibodies were labelled with corresponding fluorescently conjugated secondary antibodies, nuclei were stained with 4',6-diamidino-2-phenylindole (DAPI), and the cells were washed and examined under a fluorescence microscope (Olympus IX81, Japan).

2.4 Fluorescence-based cell proliferation assay

hPSC-CM proliferation was measured with a CyQUANT Direct Cell Proliferation Assay Kit (Invitrogen, Cat# C35011). Briefly, cell nucleic acids were stained with a green fluorescent probe, and fluorescence intensity was measured 60 min later with a microplate reader.

2.5 Measurement of ATP, NAD⁺, NADH, and cAMP levels

ATP content was measured with a luminescent ATP detection Assay kit (ab113849; Abcam) as directed by the manufacturer's protocol, and total protein content was measured via protein assay (23227, ThermoFisher); then, ATP measurements were normalized protein content. Total NAD⁺ and NADH levels were measured with a colorimetric kit (ab65348; Abcam) as directed by the manufacturer's instructions; then, the NAD⁺/NADH ratio was calculated. cAMP content was measured with a direct cAMP ELISA kit (Enzo Life Sciences) as directed by the manufacturer's instructions and normalized to the total protein content.

2.6 hCMP fabrication

hPSC-derived cardiac cells (3TCC-hCMPs: 1.4 million hPSC-CMs, 0.2 million hPSC-AECs, and 0.2 million hPSC-SMCs; 4TCC-hCMPs: 1.4 million hPSC-CMs, 0.2 million hPSC-AECs, 0.2 million hPSC-SMCs, and 0.2 million hPSC-CFs) were suspended in 0.20 mL fibrinogen solution (0.12 mL fibrinogen, 25 mg/mL, Sigma-Aldrich; 0.02 mL growth factor reduced Matrigel, Corning, and 0.56 mL HEPES, 20 mM, pH 7.4, Corning); then, the cell-containing fibrinogen solution was mixed with thrombin solution (0.004 mL thrombin, 80 U/mL, MP Biomedicals; 0.001 mL CaCl₂, 2 M, and 0.3 mL DMEM high glucose, Gibco) in a mould (internal dimensions: 1 cm x 1 cm; height: 2 mm) that had been precoated with 5% pluronic. The mixture solidified within a few minutes, and then culture medium (10% FCS, 2% B27 plus insulin, 2 mg/mL ϵ -aminocaproic acid, 10 μ M ROCK inhibitor in DMEM medium) was added to the mould and the dish. Twenty-four hours later, the culture medium was replaced with DMEM containing 2% FCS, 2% B27 plus insulin, and 2 mg/mL ϵ -aminocaproic acid, and the patches were cultured at 37°C on a rocking (45 rpm) platform for 14 days. 14,24 The culture medium was changed every

2 days, and synchronous beating of hPSC-CMs across the entire patch typically appeared on the second day after patch fabrication. hCMPs were trimmed to $0.5 \text{ cm} \times 0.6 \text{ cm} \times 2 \text{ mm}$ before transplantation into mice.

2.7 hCMP characterization

Intact hCMPs were fixed and immunostained via standard techniques.²⁴ Briefly, hCMPs were blocked and permeabilized in 10% donkey serum, 10% Tween-20, 3% BSA, 0.05% Triton X in Dulbecco's phosphate-buffered saline (DPBS) overnight at 4°C and then incubated with primary antibodies against α-SMA (Sigma-Aldrich, USA), cardiac troponin T (cTnT, Abcam, USA), clone TE-7 fibroblast antibody (TE-7, Sigma-Aldrich, USA), and CD31 (Abcam, USA) overnight at 4°C and with fluorescently labelled secondary antibodies and DAPI overnight at 4°C. The hCMPs were covered with VECTASHIELD Antifade Mounting Medium and imaged via confocal laser scanning.

2.8 Cellular composition, apoptosis, and necrosis

The hCMP was frozen in optical cutting temperature (OCT) compound and cut into 10 µm sections. Cellular composition was measured based on the immunofluorescence (IF) staining for the surface marker of each cell type (cTnT, α-SMA, CD31, TE-7) and was quantified as the ratio of the number of each cell type to total DAPI per high-power field. Apoptosis was detected with an In-situ Cell Death Detection Kit (Roche Applied Science, Germany) as directed by the manufacturer's instructions. For analysis of necrosis, sections were stained with primary rabbit antiphosphorylated mixed lineage kinase domain-like (anti-pMLKL, Cell Signaling, USA), with Alexa Fluor ® 488-conjugated phalloidin (ThermoFisher Scientific, USA), and with fluorescently conjugated secondary antibodies. Both the total number of cells and the number of TUNEL⁺ or p-MLKL⁺ cells were determined, and then apoptosis and necrosis were quantified as the ratio of the number of TUNEL⁺ and p-MLKL⁺ nuclei, respectively, to the total number of nuclei per high-power field. Analyses were performed with Image| software.

2.9 Optical mapping of membrane potential

hCMPs were stained with $5 \mu M$ of the voltage-sensitive dye RH-237,²⁴ transferred to a perfusion chamber that had been mounted on an inverted microscope, perfused with Hank's balanced salt solution at 37°C, and stimulated with 2 ms rectangular pulses delivered from a small bipolar electrode. RH-237 fluorescence was excited at 560/55 nm and measured at >650 nm. The optical signal was recorded with a 16×16 photodiode array (Hamamatsu) at a spatial resolution of 110 µm per diode as previously described 14,25 and digitally filtered to increase the signal-to-noise ratio. Activation times were measured at 50% of the maximum action-potential amplitude and used to construct the isochronal maps of activation spread. Conduction velocity (CV) was calculated from the activation time at each recording site and averaged across the whole map. The durations of the action potentials were measured at 50% (APD₅₀) and 80% (APD₈₀) of signal recovery.

For assessments in isolated hPSC-CMs, the cells were obtained from hCMPs after 7 days of culture 17 and 0.6×10^6 isolated hPSc-CMs were seeded as a monolayer on fibronectin-coated, 24-well, CytoView MEA plates (Axion Biosystems); 24-48 h later, field potential and contractility measurements were collected on a Maestro Edge apparatus (Axion Biosystems) and analysed by using the Cardiac Module in Axion Navigator software.²⁶ Action-potential durations (APDs) were determined via the LEAP assay and characterized with the Cardiac Analysis Tool.

2.10 Quantitative reverse transcription polymerase chain reaction

Total RNA was extracted by using Qiashredder and RNeasy mini kits (Qiagen, USA) as directed by the manufacturer's instructions, and the

mRNA concentration was measured with a NanoDrop 1000 Spectrophotometer. RNA (1 µg per 20 µL reaction) was reverse transcribed with SuperScript II Reverse Transcriptase (Thermo Scientific, USA) and appropriate primers (Table 1), and quantitative reverse transcription polymerase chain reaction (qRT-PCR) was performed with Maxima SYBR Green Master Mix (Thermo Scientific) on a Realplex2 Real-Time PCR system (Eppendorf, USA). Measurements were normalized to the level of endogenous glyceraldehyde phosphate dehydrogenase (GAPDH) RNA.

(GAPDH) RNA. **2.11** In vitro angiogenesis array

The expression of angiogenesis-related proteins was measured using a Human Angiogenesis Antibody Array O 1000 (RayBiotech. Inc. C.) Human Angiogenesis Antibody Array O 1000 (RayBiotech, Inc., Norcross GA, USA) according to the manufacturer's protocols. It is a combination of Human Angiogenesis Array Q2 & Q3 and detects 60 human angiogenic factors. Measurements were made using supernatants from 3 displayed biological samples (two technical replicates each) of 3TCC- or 4TCC-hCMPs after 48 h of serum-free (Basel DMEM medium only) aculture.

2.12 Mouse MI model

All animal procedures were performed in accordance with the guidelines for animal experimentation set forth and approved by the Institutional Animal Care and Use Committee (IACUC, APN 20502), School of Engineering, University of Alabama, Birmingham, and conformed to the Guidelines for the Care and Use of Laboratory Animals published by the US National Institutes of Health (2011) (NIH publication No 85-23). The number of animals for each group was calculated according to our previous study²⁵ and Rosner's equation 27,28 using values for power = 0.80 and $\frac{1}{2}$ significance level = 0.05. According to this calculation, minimum 6 mice are $\frac{3}{2}$ required for each group. All data are analysed with analysis of variance $\frac{1}{100}$ (ANOVA). A value of P < 0.05 is considered significant. Surgical induction of MI was performed in 8- to 10-week-old NOD/SCID gamma mice [NOD.Cg-Prkdc^{scid}ll2rg^{tm1Wjl}/SzJ (005557); The Jackson Laboratory]; 6-11 animals were included in each treatment group. 25,29 Briefly, mice were intubated, connected to a ventilator, and anesthetized with inhaled $^{\infty}_{80}$ 1–1.5% isoflurane USP (FlurisoTM, VetOne®). The heart was exposed $^{\infty}_{80}$ via a left thoracotomy, and MI was induced by permanently ligating the E left anterior descending (LAD) coronary artery with a non-absorbable suture; sham surgery was performed via the same protocol, including passage of the suture around the LAD artery, but the artery was not ligated. The 3TCC-hCMP or 4TCC-hCMP was applied after arterial ligation, and animals in the Sham and MI-only groups recovered without either experimental treatment. The chest was closed, and intraperitoneal injections of ਰੋ buprenorphine hydrochloride (0.1 mg/kg every 12 h for up to 3 days after surgery; Buprenex®, Reckitt Benckiser Pharmaceuticals Inc.) and carprofen (5 mg/kg every 12 h for 1 day after surgery; Rimadyl®, Zoetis) were provided for pain control. For euthanasia, mice were anesthetized with inhaled 5% isoflurane for several minutes; then, anaesthesia was confirmed via tail pinch, and cervical dislocation was performed before chest incision \sqrt{g} and heart removal.

2.13 Echocardiography

Echocardiographic imaging was performed as previously described. 25,29 Briefly, animals were maintained under 1-1.5% isoflurane USP (FlurisoTM, VetOne®) anaesthesia, and parasternal long-axis and twodimensional short-axis images were acquired with a high-resolution microultrasound system (Vevo 2100, VisualSonics, Inc.). Data were analysed and LV ejection fraction (EF) and fractional shortening (FS) were calculated with Vevo analysis software. The operator was blind to the experimental groups.

2.14 Engraftment rate

Engraftment was determined via IF analyses in cryopreserved heart sections.²⁵ Briefly, coronal sections were cut from apex to base at 10 µm

Table 1 Reverse transcription-quantitative real-time polymerase chain reaction primer sequences used in this study

Genes	Forward primer	Reverse primer	Product length (bp)	Annealing temperature (°C)
GAPDH	TCGACAGTCAGCCGCATCTTCTTT	ACCAAATCCGTTGACTCCGACCTT	94	58
TNNI1	GGTGGATGAGGAGCGATACG	GCTTCAGGTCCTTAATCTCCCTG	71	58
TNNI3	CCTCACTGACCCTCCAAACG	GAGGTTCCCTAGCCGCATC	104	58
TNNT2	TTCACCAAAGATCTGCTCCTCGCT	TTATTACTGGTGTGGAGTGGGTGTGG	165	58
MYH6	CTCCGTGAAGGGATAACCAGG	TTCACAGTCACCGTCTTCCC	248	58
MYH7	ACCGTCCCCGCTCCTTC	TCATTCAAGCCCTTCGTGCC	131	58
MLC2v	ACATCATCACCCACGGAGAAGAGA	ATTGGAACATGGCCTCTGGATGGA	164	58
MLC2a	GGAGTTCAAAGAAGCCTTCAGC	AAAGAGCGTGAGGAAGACGG	178	58
PPARA	GCTTTCTGGGTGGACTCAAGT	GAGGGCAATCCGTCTTCATCC	175	58
COX6A2	CATCCGCACCAAGCCCTAC	CCTTTATTGTGTCCGGGGGC	127	58
CKMT2	GCTCCGGCTTCAAGACACTC	TGCGCTTGGAGGAAATAGCC	190	58
SERCA 2	TCACCTGTGAGAATTGACTGG	AGAAAGAGTGTGCAGCGGAT	149	58
RYR2	TTGGAAGTGGACTCCAAGAAA	CGAAGACGAGATCCAGTTCC	141	58
NCX1	CCCGTCTGGTGGAGATGAGTGAGAA	TTGCTGGTCAGTGGCTGCTTGTC	172	58
Cx43	TGAGCAGTCTGCCTTTCGTT	CCAGAAGCGCACATGAGAGA	94	58
KCNJ2	TGCGCCAGCAACAGGACAT	GTGTCTCTGGGAGCCTTGTG	105	58

intervals, and every 30th serial section was stained with antibodies for cTnT, human-specific cTnT (hcTnT), and human nuclear antigen (HNA; Abcam, USA). hcTnT-expressing cells were counted, and the total was multiplied by 15 to calculate the number of engrafted hPSC-CMs per heart. hPSC-CM engraftment was calculated as the ratio of hcTnT+ cells to the number of hPSC-CMs in the implanted hCMP. The engraftment of hPSC-derived non-CM cells was calculated as the ratio of the number of cells that were both hcTnT- and HNA+ to the number of transplanted hPSC-derived non-CM cells.

2.15 Infarct size

Excised hearts were fixed in 4% PFA for 24 h, dehydrated, cleared, and embedded in OCT compound for cryopreservation; then, infarct size was calculated as described previously. Coronal sections were cut from apex to base at 10 μm intervals; then, every 30th serial section was fixed in Bouin's solution, and stained with 0.04% Sirius Red to label the myocardial scar and with 0.1% Fast Green to label the uninjured myocardial tissue. Digital images of the stained sections were captured via light microscopy and analysed with NIH ImageJ 20 software. The length of collagen deposition (red) and the total length of the LV were measured, and the scar size was calculated with the following formula: Scar size = (Sum of the scar length from all sections \times thickness of section) \div (Total length of LV from all sections \times thickness of section) \times 100%. 25

2.16 Vascular density

Vascular density was evaluated in cryopreserved sections as described previously. 14,25,29 Briefly, sections were immunofluorescently stained with wheat germ agglutinin (WGA) and isolectin B4 (IB4), and vascular density was quantified as the number of positively stained vessel-like structures per unit area.

2.17 Statistical analysis

All assessments were conducted by an investigator who was blinded to the experimental condition and/or treatment group. Statistical analyses were conducted with a minimum of three samples per group, and data are presented as mean \pm standard error mean (SEM). Significance (P < 0.05) was determined via the Student's t-test for comparisons between two groups, and one-way or two-way ANOVA for comparisons among three or more groups.

3. Results

3.1 hPSC-CMs, -SMCs, -AECs, and -CFs expressed the corresponding lineage markers

hPSCs were differentiated into hPSC-CMs, -SMCs, -AECs, and -CFs as previously reported, 1,3,4,19 and subsequent assessments confirmed the expression of appropriate lineage markers in each differentiated cell type: hPSC-CMs expressed cardiac troponin T (cTnT), α -actinin, and N-cadherin; hPSC-SMCs expressed α -SMA, smooth muscle 22 α $[SM22\alpha]$, and calponin 1; hPSC-AECs expressed CD31, VE-cadherin, and VWF; and hPSC-CFs expressed fibroblast antibody clone TE-7 (TE-7) and vimentin, but not the myofibroblast markers α -SMA and calponin 1 (Figure 1). In vitro experiments with cultured hPSC-CMs confirmed that the cells essentially have a limited proliferation rate (Supplemental material online, Figure S1), and flow cytometry analyses indicated that each of the final hPSC-derived cell populations was at least 97% pure: 97.6% of hPSC-CMs expressed cTnT, 98.2% of hPSC-SMCs expressed α-SMA, >99% of hPSC-AECs expressed CD31 or VE-cadherin (CD144), and 99.4% of hPSC-CFs expressed TE-7 (Supplemental material online, Figure S2).

3.2 4TCC-hCMPs developed a more mature sarcomeric structure when cultured on a rocking platform

hCMPs (1 cm \times 1 cm \times 2 mm) were fabricated by mixing a cell-containing fibrinogen solution with thrombin in a mould. Both 3TCC- and 4TCC-hCMPs were constructed with 1.4 million hPSC-CMs, 0.2 million hPSC-SMCs, and 0.2 million hPSC-AECs, and the 4TCC-hCMPs contained an additional 0.2 million hPSC-CFs; thus, a total of 2 million cells were included in the 4TCC-hCMPs, while the 3TCC-hCMPs contained 1.8 million cells. After 3 or 14 days of culture on a rocking (45 rpm) platform, hPSC-derived cardiac cells were identified in the hCMPs via IF staining for lineage-marker expression (hPSC-CMs: cTnT, hPSC-SMCs: α -SMA, hPSC-AECs: CD31, hPSC-CFs: TE-7) on the cross section of hCMPs or intact hCMPs. The proportion of cells expressing each lineage marker on Day 14 was equivalent to the cellular composition seeded for hCMP fabrication (Figure 2, Supplemental material online, Figure S5, Table 2), which

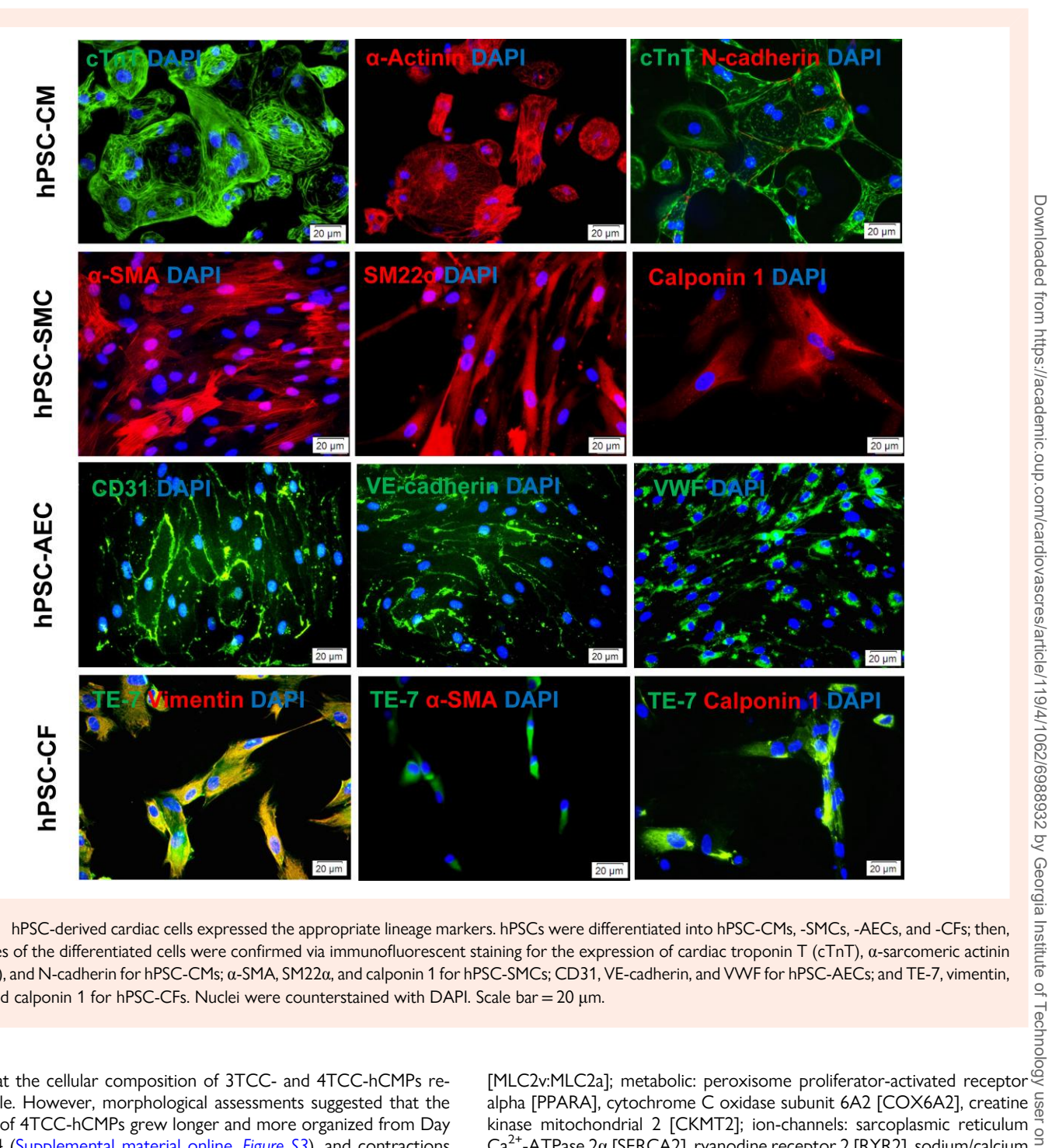


Figure 1 hPSC-derived cardiac cells expressed the appropriate lineage markers. hPSCs were differentiated into hPSC-CMs, -SMCs, -AECs, and -CFs; then, the lineages of the differentiated cells were confirmed via immunofluorescent staining for the expression of cardiac troponin T (cTnT), α-sarcomeric actinin $(\alpha$ -Actinin), and N-cadherin for hPSC-CMs; α -SMA, SM22 α , and calponin 1 for hPSC-SMCs; CD31, VE-cadherin, and VWF for hPSC-AECs; and TE-7, vimentin, α -SMA, and calponin 1 for hPSC-CFs. Nuclei were counterstained with DAPI. Scale bar = 20 μ m.

confirms that the cellular composition of 3TCC- and 4TCC-hCMPs remained stable. However, morphological assessments suggested that the sarcomeres of 4TCC-hCMPs grew longer and more organized from Day 3 to Day 14 (Supplemental material online, Figure S3), and contractions were notably stronger in 4TCC- than in 3TCC-hCMPs at the later time point (Supplemental material online, Movies 1 and 2). The proportion of apoptotic (positive TUNEL staining) and necrotic [positive staining for phosphorylated mixed lineage kinase domain-like (pMLKL)] hPSC-CMs in 4TCC- and 3TCC-hCMPs was similar (Figure 3).

3.3 hPSC-CFs promoted hCMP maturation

Whether hPSC-CFs can improve the maturation of cultured hCMPs was investigated by comparing the patterns of expression for structural, metabolic, and ion-channel marker proteins that are associated with CM maturation (structural: human cTnT [TNNT2] and the ratios of cardiac: slow-skeletal Tnl isoforms [TNNI3:TNNI1], myosin heavy chain isoforms 7:6 [MYH7:MYH6], and the myosin light chain 2 ventricular:atrial isoforms

alpha [PPARA], cytochrome C oxidase subunit 6A2 [COX6A2], creatine 🗑 kinase mitochondrial 2 [CKMT2]; ion-channels: sarcoplasmic reticulum Ca^{2+} -ATPase 2α [SERCA2], ryanodine receptor 2 [RYR2], sodium/calcium exchanger 1 [NCX1], Connexin 43 [Cx43], and cardiac inward rectifier potassium channel [KCNJ2]). When evaluated via qRT-PCR, measurements of mRNA abundance (Figures 4A-C), all markers were significantly greater in 4TCC-hCMPs than in 3TCC-hCMPs. 4TCC-hCMPs also had significantly greater amounts of cTnT, cTnl, and Cx43 protein (Figures 4D and E), higher ATP and cAMP levels, and a greater ratio of NAD+ to NADH (Figure 4F and G). Recent studies indicated that increased intracellular cAMP level in hPSC-CMs is associated with the involvement of hPSC-CFs¹⁷ in a study using cardiac microtissues examining the metabolic maturation of hPSC-CMs. ¹⁷ The results in Figure 4 demonstrate that the cAMP level was significantly increased in 4TCC-hCMPs compared with 3TCC-hCMPs (Figure 4H). The change of cAMP levels in 4TCC-hCMPs was also accompanied by a significant increase in measurements of mRNA expression of PGC- 1α , which is a downstream targeted gene of

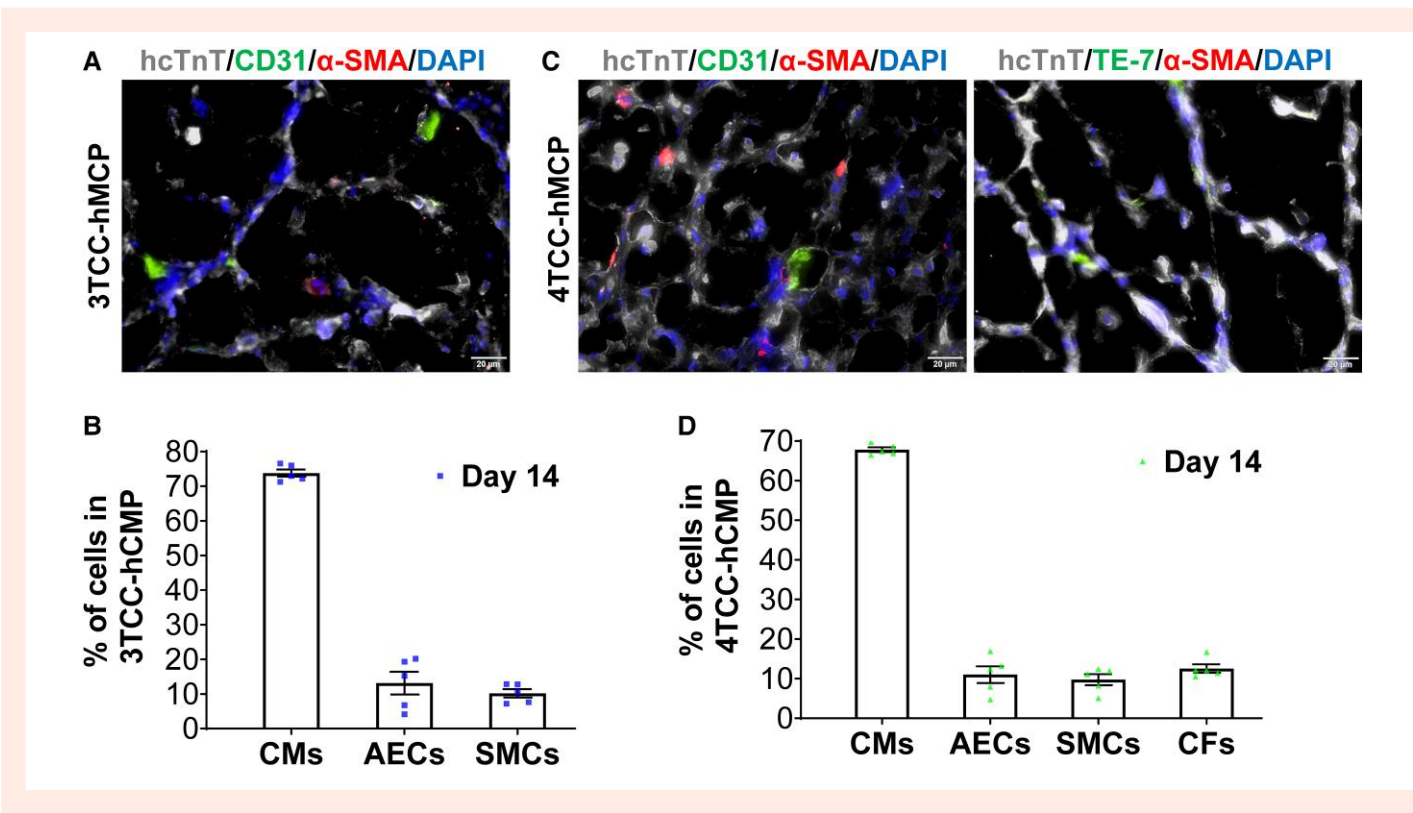


Figure 2 Cellular composition of hCMPs was stable for at least 14 days in culture. (A) hPSC-CMs, -AECs, and -SMCs were identified in 3TCC-hCMPs via IF staining for the presence of hcTnT, CD31, and α-SMA, respectively; then, (B) the percentage of cells that stained positively for each marker was calculated. (C) hPSC-CMs, -AECs, -SMCs, and -CFs were identified in 4TCC-hCMP via IF staining for the presence of hcTnT, CD31, α-SMA, or TE-7, respectively; then, (D) the percentage of cells that stained positively for each marker was calculated. Scale bar = 20 μM (n = 5).

cAMP. PGC-1 α is a transcriptional co-regulator that promotes CM maturation and regulates mitochondria carbon substrate preference of ATP production towards using more fatty acids than glucose in oxidative phosphorylation, ^{31,32} which again suggests that the hiPSC-CF in hCMP promotes the CM maturation.

Furthermore, although optical-mapping measurements of time to 50 and 90% of action-potential recovery (APD₅₀ and APD₉₀, respectively) did not differ significantly in 4TCC- and 3TCC-hCMPs (*Figure 5D* and *E*), the CV (*Figure 5A*–C) showed a significant increase in 4TCC-hCMPs in comparison to 3TCC-hCMPs. In addition, all three parameters were significantly greater in hPSC-CMs isolated from 4TCC-hCMPs than in hPSC-CMs from 3TCC-hCMPs (*Figure 5F–J*). Thus, the inclusion of hPSC-CFs during patch manufacture appeared to promote the structural, metabolic, bioenergetic, and electrophysiological maturation of hCMPs.

3.4 hiPSC-FBs changed the profile of angiogenic factors released from 4TCC as compared with 3TCC patches

The angiogenic factors released from 3TCC and 4TCC patches were shown in Supplementary material online, Tables S1 and S2. When evaluated using the Human Angiogenesis Array, the abundance of Activin-A, angiopoietin-2, angiopoietin-like 4, basic FGF, epithelial neutrophilactivating peptide, hepatocyte growth factor, IL-1 α , IL-1 β , IP-10, LIF, placental growth factor, RANTES, CXCL16, MCP-2, MCP-3, MMP-9, PECAM-1, uPAR, I-TAC, and VEGFR2 were greater, whereas TIMP-1, TIMP-2, TPO, FGF-4, and TGF- α were less abundant, in the medium from 4TCC than from 3TCC patches.

3.5 The inclusion of hPSC-CFs during manufacture increased the potency of hCMPs for myocardial repair in mice

The effectiveness of 4TCC- and 3TCC-hCMPs for promoting cardiac recovery was compared in a murine MI model. MI was induced via permanent ligation of the LAD coronary artery, and then animals in the 4TCC-hCMP group were treated with 4TCC-hCMPs; animals in the 3TCC-hCMP group were treated with 3TCC-hCMPs; and animals in the MI-only group recovered without either experimental treatment. Both hCMP constructs were trimmed to 0.5 cm \times 0.6 cm \times 2 mm before implantation; thus, the total number of administered cells was 0.6 million and 0.54 million in the 4TCC- and 3TCC-hCMP treatment groups, respectively.

Echocardiographic assessments (Figure 6A) of LVEF (Figure 6B) and LVFS (Figure 6C) were equivalent in all three groups before MI but significantly greater in 4TCC-hCMP animals than in either the 3TCC-hCMP or MI-only groups 7 and 28 days afterward. LVEF, LVFS, and the thickness of the LV anterior wall (Supplemental material online, Figure S6A and B) were also significantly greater in 3TCC-hCMP than in MI-only animals on Day 28, and measurements appeared to increase (but not significantly) between the two time points in both hCMP treatment groups, whereas measurements in MI-only animals declined. Infarcts were also significantly smaller in hearts explanted from 4TCC-hCMP than from 3TCC-hCMP or MI-only animals on Day 28 (Figures 6D and E), whereas heart-weight: bodyweight ratios were significantly lower in 4TCC-hCMP than in 3TCC-hCMP-treated animals and in both hCMP treatment groups than in MI-only animals (Supplemental material online, Figure S4).

Table 2 Cellular c	composition of	f patches
--------------------	----------------	-----------

Name	Composition	CMs	AECs	SMCs	CFs	Total cell number
3TCC-hCMP	%	77.80%	11.10%	11.10%	-	0.54 million
	Cell number	0.42 million	0.06 million	0.06 million	-	
4TCC-hCMP	%	70%	10%	10%	10%	0.6 million
	Cell number	0.42 million	0.06 million	0.06 million	0.06 million	

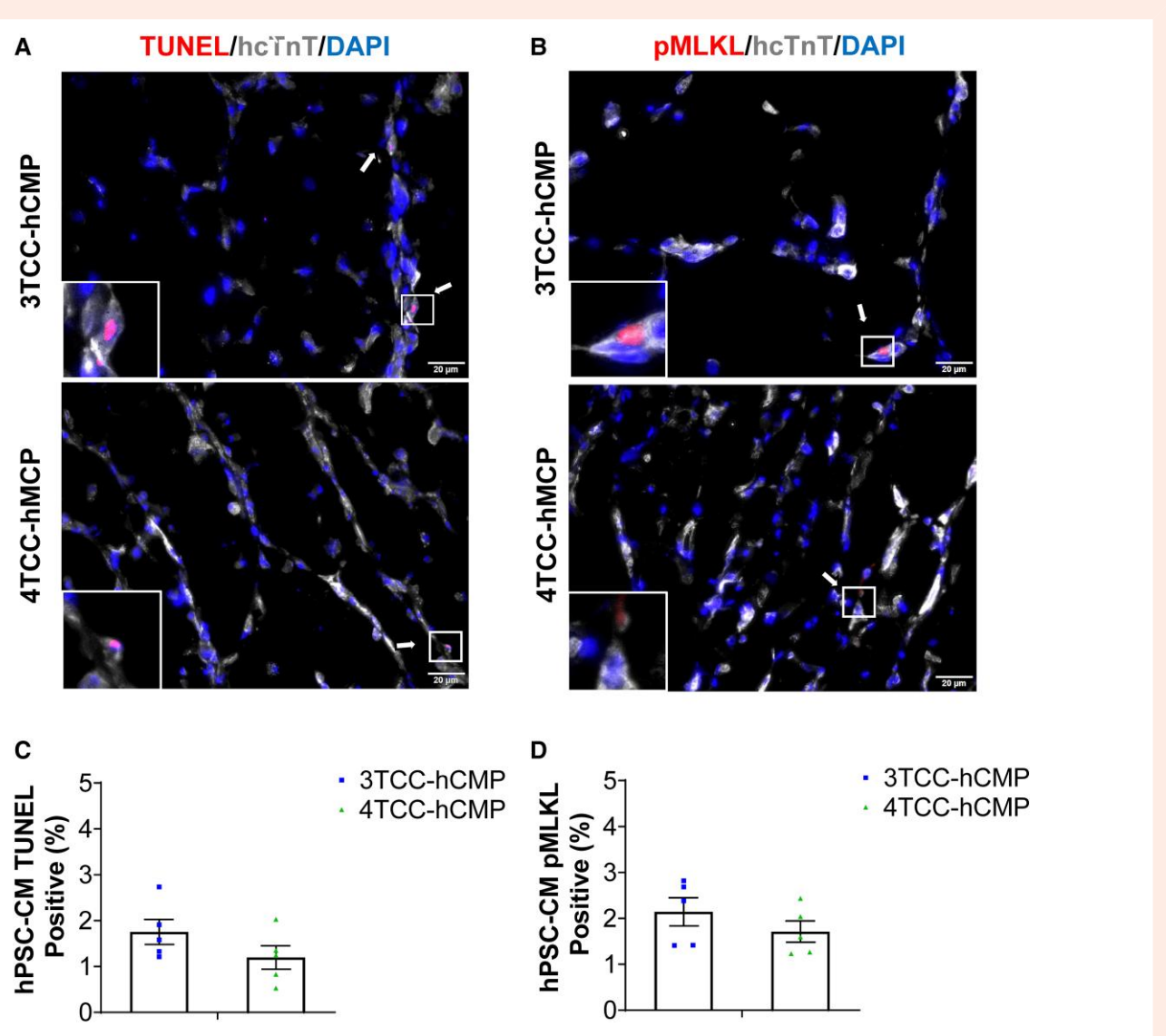
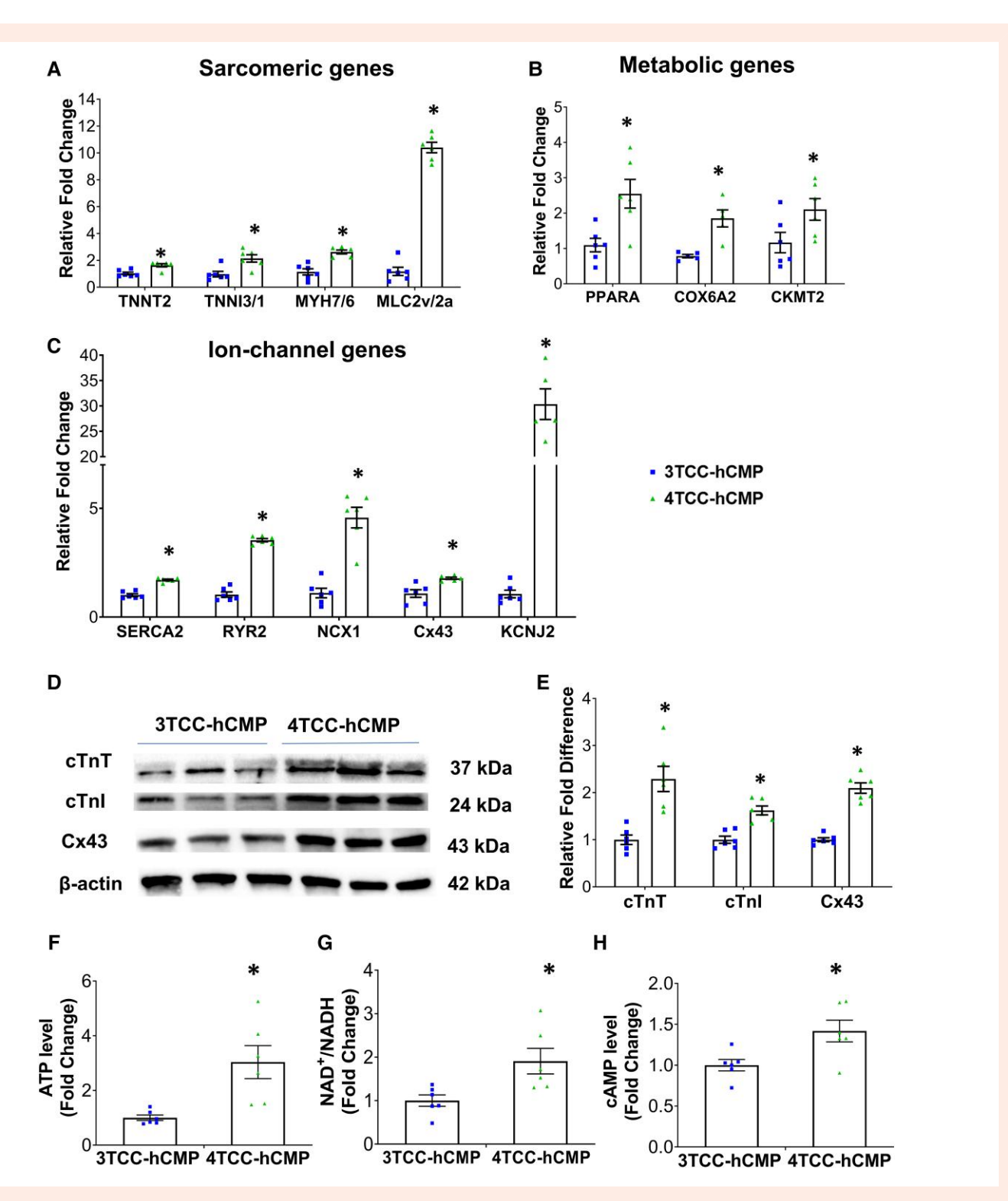


Figure 3 Necrotic and apoptotic hPSC-CMs were uncommon in 3TCC- and 4TCC-hCMPs. After 14 days of culture, hPSC-CMs were identified in 3TCC- and 4TCC-hCMPs by staining for hcTnT expression; then (A) apoptotic and (B) necrotic cells were identified via terminal deoxynucleotidyl transferase dUTP nick-end labelling (TUNEL) and immunofluorescent staining for pMLKL, respectively. (C) Apoptosis was quantified as the percentage of TUNEL $^+$ cells, and (D) necrosis was quantified as the percentage of pMLKL-positive cells. Nuclei were counterstained with DAPI. Scale bar = 20 μ m.

3.6 hPSC-CM engraftment was greater in 4TCC-hCMP-treated hearts than in hearts treated with 3TCC-hCMPs

Because the hCMPs were generated with human cells, cells from the implanted hCMPs were identified in heart sections by immunofluorescently staining for expression of the human isoform of cTnT (hcTnT) and HNA

(Figure 7A). The engraftment of hPSC-CMs (Figure 7B) was significantly greater in animals treated with 4TCC-hCMPs than in 3TCC-hCMP animals, but the engraftment of non-CMs did not differ significantly between the two treatment groups (Figure 7C). Furthermore, when vascularity was evaluated by staining sections from the border zones of infarction with IB4 and WGA (Figure 7D), the density of positively stained vessels was greater in sections from both hCMP-treated groups than from MI-only animals and



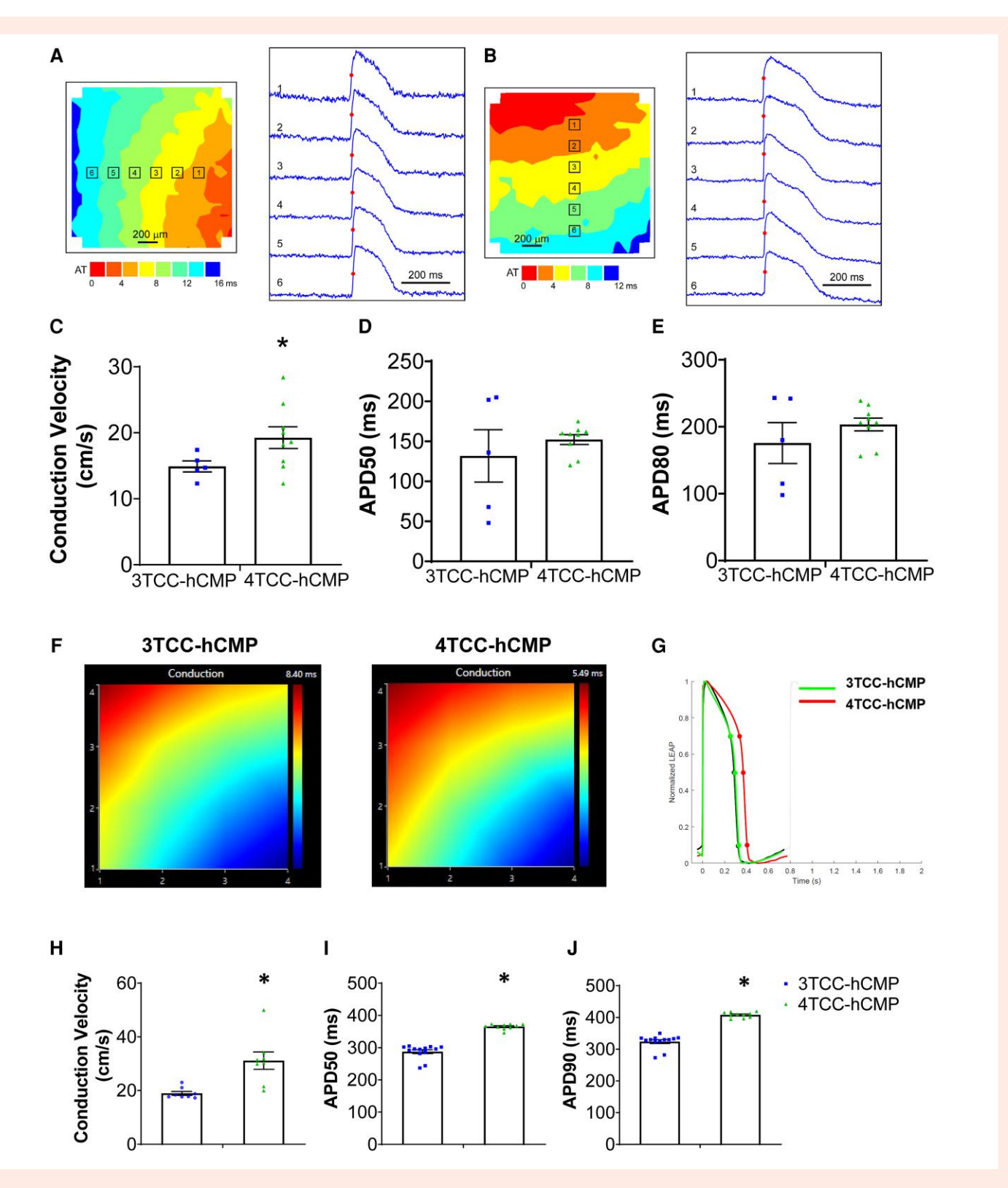


Figure 5 Conduction velocity (CV) and action-potential durations were greater in hPSC-CMs isolated from 4TCC- than from 3TCC-hCMPs. Optical maps of action-potential propagation were constructed after 7 days of culture for (A) 3TCC- and (B) 4TCC-hCMPs that had been stained with a voltage-sensitive dye (cycle length = 490–800 ms). (C) CV was calculated from the activation time at each recording site and averaged across the whole map, and the durations of the action potentials were measured at (D) 50% (APD50) and (E) 90% (APD90) of signal recovery. hPSC-CMs were isolated from hCMPs after 7 days of culture, seeded on fibronectin-coated, 24-well, microelectrode array plates, and analysed 24–48 h later. (F) Optical maps of action-potential propagation and (G) action-potential traces were collected for hPSC-CMs isolated from 3TCC- and 4TCC-hCMPs (pacing = 1.25 Hz, cycle length = 800 ms). (H) CVs and action-potential durations until (I) 50% (APD50) and (J) 90% (APD90) recovery were calculated (pacing = 1.25 Hz, cycle length = 800 ms). *P < 0.05 vs. 3TCC-hCMP, Student's t-test (n = 5-13).

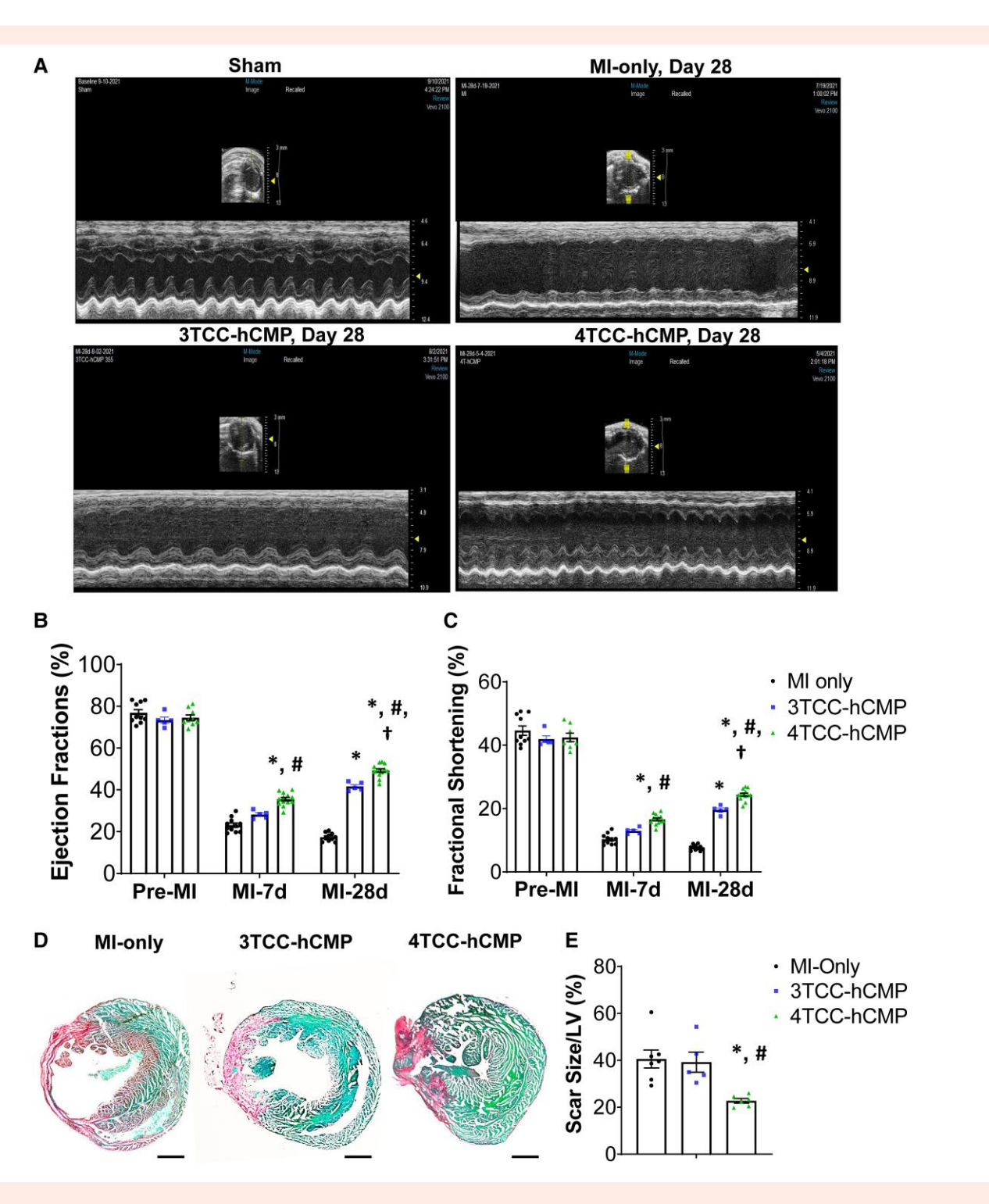


Figure 6 4TCC-hCMPs were more potent than 3TCC-hCMPs for improving recovery from MI in mice. MI was induced in mice, and then animals were treated with 3TCC-hCMPs, with 4TCC-hCMPs, or without either experimental treatment (MI-only). A fourth group of animals underwent Sham surgery and also recovered without either experimental treatment. (A) Echocardiographic images were obtained (B-C) before MI induction (Pre-MI) and 7 and 28 days afterward (MI-7d and MI-28d, respectively) and used to calculate measurements of (B) LVEF and (C) LVFS. (D) Sections from the LV of animals sacrificed on Day 28 were stained with Sirius Red (fibrotic tissue, pink-red) and Fast Green (non-fibrotic tissue, blue-green), and then (E) the scar size was evaluated as the percentage of the LV surface area that was fibrotic. *P < 0.05 vs. MI-only, *P < 0.05 vs. 3TCC-hCMP, *P < 0.05 vs. same group on Day 7. Panel A: The dashed line in Figure 6A indicates the diameter of mouse heart at short-axis. Panels B and C: two-way ANOVA with Tukey's multiple comparisons test (n = 5–12); Panel E: one-way ANOVA with Tukey's multiple comparisons test (n = 5–12). Scale bar = 1 mm.

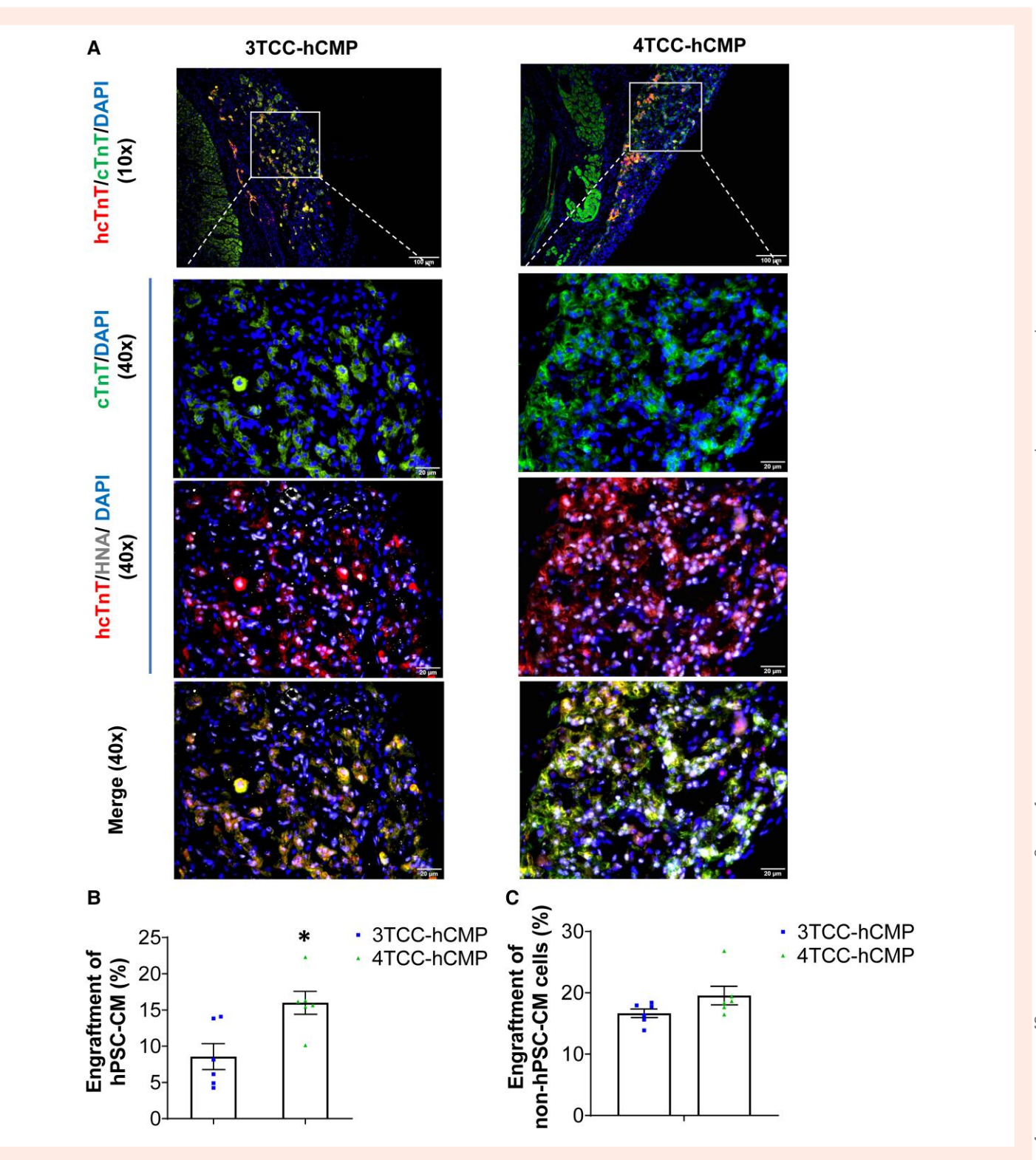
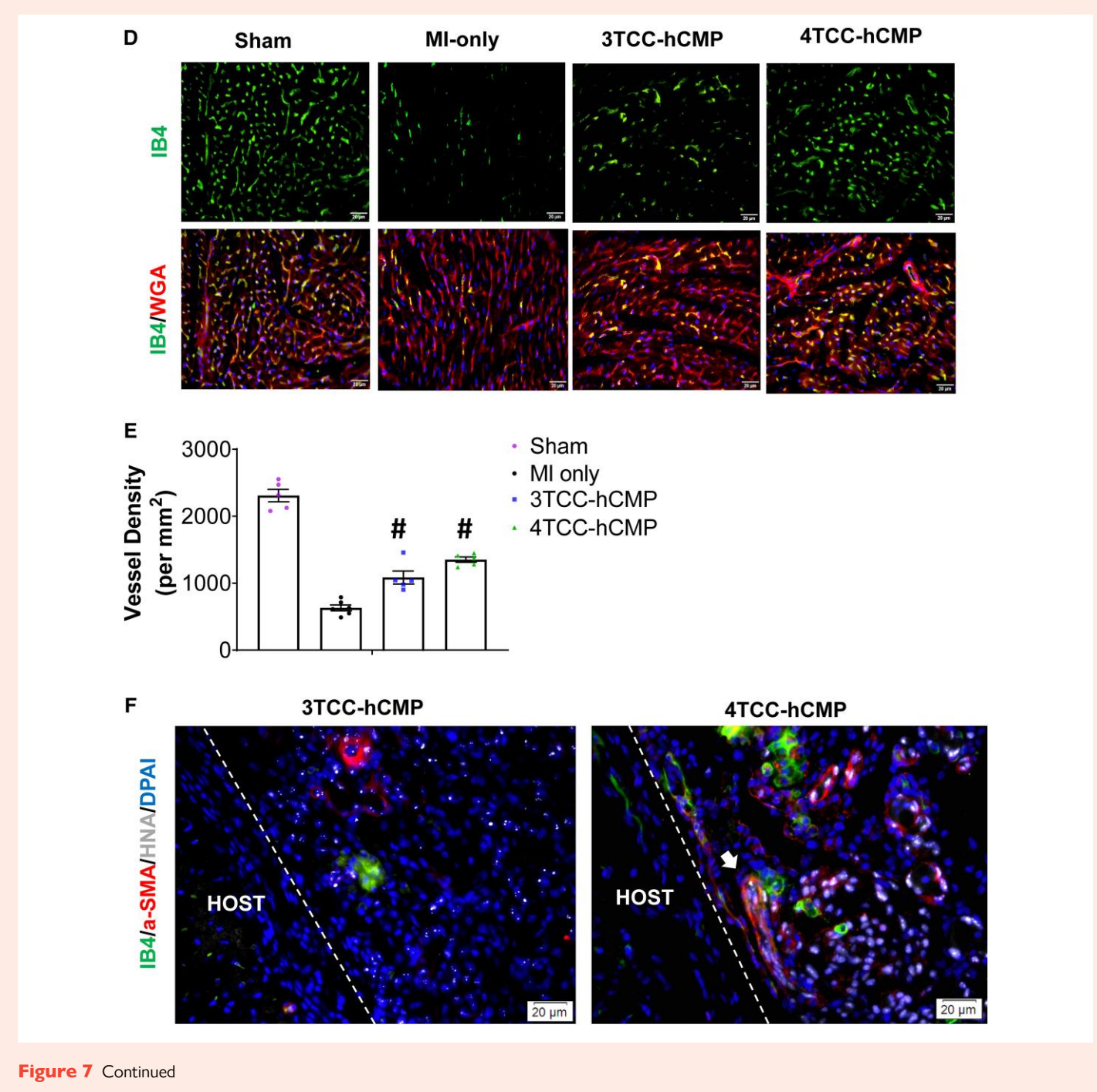


Figure 7 hPSC-CM engraftment was significantly greater in 4TCC-hCMP-treated hearts than in hearts treated with 3TCC-hCMPs. (A) Sections from the region of 3TCC- or 4TCC-hCMP transplantation were immunofluorescently stained for the expression of cTnT, the hcTNT, and HNA. (B) hPSC-CM engraftment was calculated as the ratio of hcTNT+ cells to the total number of hPSC-CMs in the hCMP and presented as a percentage. (C) The engraftment of hPSC-derived non-CMs was calculated as the ratio of cells that were both HNA+ and hcTNT− to the total number of hPSC-derived non-CMs in the hCMP and presented as a percentage. (D) Sections from the infarcted zone in hearts from animals in the 3TCC-hCMP, 4TCC-hCMP, and MI-only groups, and from the corresponding region of hearts from Sham animals, were immunofluorescently stained with WGA and IB4; then, (E) vessel density was quantified as the number of IB4-positive vascular structures per square millimetre. (F) Arterioles containing cells from the transplanted hCMPs (arrows) were visualized in sections from the hearts of 3TCC- and 4TCC-hCMP animals via immunofluorescent staining for IB4, HNA, and α-SMA; nuclei were counterstained with DAPI. *P < 0.05 vs. 3TCC-hMCP, *P < 0.05 vs. MI-only. *P <



in the 4TCC-hCMP group than in 3TCC-hCMP animals (*Figure 7E*), but the differences between the groups did not reach statistical significance. Notably, cells expressing IB4, but not HNA, were observed in the region of hCMP implantation (*Figure 7F*), which suggests that native vessels had grown from the surrounding myocardium into the hCMP, but we observed

no evidence that hPSC-derived cells had migrated from the hCMP into the injured ventricular wall.

4. Discussion

The ongoing development of hPSC technology has spurred considerable advancement in the fabrication of engineered myocardium for repairing the damage caused by myocardial injury.^{14,33,34} Previously, we have shown

that when cultured under dynamic conditions, hCMPs composed of hPSC-CMs, -SMCs, and -ECs suspended in a fibrin matrix (3TCC-hCMPs) were associated with improvements in cardiac function, infarct size 4 weeks after administration to infarcted pig hearts.³⁵ In the present study, we hypothesized that the addition of hiPSC-CFs may further improve the efficacy, which may be partially attributable to the improvement of the maturation of hPSC-CMs.^{17,36,37}

The 4TCC-hCMPs became progressively more mature during the culture period, as evidenced by improvements in structural anisotropy and myofilament alignment, and the expression of CM maturation markers was significantly greater in 4TCC-hCMPs than in 3TCC-hCMPs when evaluated via IF staining, qRT–PCR, and western blot. Ion-channel protein abundance, markers for metabolic maturity, and CVs were also significantly greater in hPSC-CMs of

4TCC-hCMPs than in 3TCC-hCMPs, which suggests that the inclusion of hPSC-CFs improved the functional maturity of hPSC-CMs. Furthermore, the contractions observed in 4TCC-hCMPs were qualitatively stronger than those in 3TCC-hCMPs, and the abundance of ATP and cAMP, as well as the NAD+/NADH ratio, were significantly greater in 4TCC-hCMPs. Recent reports have emerged that increased intracellular cAMP level in hPSC-CMs is associated with the involvement of hPSC-CFs¹⁷ in a study using cardiac microtissues examining the metabolic maturation of hPSC-CMs. ¹⁷ Current study indicates that the cAMP level was significantly increased in 4TCC-hCMPs compared with 3TCC-hCMPs (Figure 4H). The change of cAMP levels in 4TCC-hCMPs was also accompanied by a significant increase in measurements of mRNA expression of PGC-1α, which is a downstream targeted gene of cAMP. PGC- 1α is a transcriptional co-regulator that promotes CM maturation and regulates mitochondria carbon substrate preference of ATP production towards more fatty acid oxidative phosphorylation.^{31,32} Results in the present study indicate that while mRNA levels of mitochondrial genes (i.e. COX6A2 and CKMT2) were up-regulated in 4TCC-hCMPs, the ATP level in CMs was significantly increased in 4TCC-hCMPs compared with 3TCC-hCMPs (Figure 4F), which is also associated with the increase of NAD⁺/NADH ratio in 4TCC-hCMPs (Figure 4G). Taken together, these results indicate that CF in 4TCC-hCMPs promotes the maturation of CMs in the engineered tissue via the enhanced intracellular cAMP signalling pathway. Collectively, these observations suggest that 4TCC-hCMPs may be functionally superior to 3TCC-hCMPs, and that much of the improvement can be attributed to the inclusion of hPSC-CFs, but direct assessments of the arrhythmogenic risk associated with 4TCC-hCMP transplantation will likely require experiments in large animals that have been implanted with loop recorders for continuous electrocardiogram monitoring.

hPSC-AECs appear to support arteriogenesis more effectively than conventional hPSC-ECs^{19,20}; thus, since both the survival of transplanted cells and the repair of damaged tissue are crucially dependent on adequate vascularity and perfusion, the hPSC-ECs incorporated into our 3TCC- and 4TCC-hCMPs were generated via a differentiation protocol that promoted the arterial EC phenotype. Measurements of engraftment were significantly greater in hearts treated with implanted 4TCC-hCMPs after MI than in 3TCC-hCMP-treated hearts, and the implanted 4TCC-hCMPs were associated with significantly better measurements of LVEF, LVFS, infarct size, and hypertrophy. However, whether (and to what extent) these improvements could be attributable to the inclusion of hPSC-AECs, or to the activity of hPSC-CFs in concert with the other types of cardiac cells in the 4TCC-hCMP, remains unclear. In addition, CFs have been demonstrated that play an important role in extracellular matrix excretion³⁸ and structural support formation in myocardium^{39,40} or engineered cardiac tissue. 41,42 Besides its paracrine contribution (Supplementary material online, Tables S1 and S2), another explanation for promoted cardiac function and reduced scar size of the 4TCC-hCMP-treated group compared with the 3TCC-hCMP-treated group could be the direct contribution to contractility by the transplanted 4TCC-hCMP, due to the mechanical support of hPSC-CFs. In this case, in order to better evaluate the mechanical performance of hCMP, the mechanical behaviour needs to be tested and compared with native heart tissue, such as contractility assay¹⁴ and stress-strain relationship analysis.⁴³ Further characterization of 4TCC-hCMPs will give us a comprehensive understanding of cellular interaction effects on its structure and function and enable us to improve the efficacy of MI therapy. Furthermore, the results from multiple studies suggest that the benefit of cell-based myocardial therapy is mediated primarily by paracrine factors that are released from the transplanted cells, including transplanted CMs, 44-46 so much of the functional improvement observed in the hearts of animals from both hCMP treatment groups likely evolved indirectly, rather than via the direct participation of hPSC-CMs in myocardial contractions.

5. Conclusion

hPSC-CFs promoted CM maturation in cultured 4TCC-hCMPs, and when evaluated in a murine MI model, assessments of cardiac function and infarct

size were significantly better after treatment with implanted 4TCC-hCMPs than in 3TCC-hCMP-treated animals. Measures of hPSC-CM engraftment were also greater in 4TCC-hCMP-treated mice, which may have been at least partially attributable to the inclusion of hPSC-CF, during hCMP manufacture. It is noted that the imaging quality of cryo-sectioning of the fibrin-based constructs is difficult. However, it is sufficient for the purpose of cell-type analysis and the quantification of apoptosis in the present study. Additional studies are warranted to characterize the mechanisms that support the enhanced potency of 4TCC-hCMPs for myocardial repair and to begin evaluating the safety and efficacy of 4TCC-hCMPs in clinically relevant, large mammal models of cardiac injury.

Supplementary material

Supplementary material is available at Cardiovascular Research online.

Authors' contribution

X.L. and J.Z. designed the study. X.L. carried out the experiments. Y.T. performed the surgery and sample collection. X.L., D.P., A.K., Jue Z., and Jh.Z. on the surgery and sample collection. X.L., D.P., A.K., Jue Z., and Jh.Z. on the surgery and sample collection. X.L., D.P., A.K., Jue Z., and Jh.Z. on the surgery and sample collection. X.L., D.P., A.K., Jue Z., and Jh.Z. on the surgery and sample collection. X.L., D.P., A.K., Jue Z., and Jh.Z. on the surgery and sample collection. X.L., D.P., A.K., Jue Z., and Jh.Z. on the surgery and sample collection. port the enhanced potency of 4TCC-hCMPs for myocardial repair and to

did cell differentiation. V.F. performed optical mapping. X.L. and J.Z. wrote the manuscript. X.L. I.Y. A.O. V.E. C.O. T.Y. T. the manuscript. X.L., L.Y., A.Q., V.F., G.Q., T.K., J.T., and J.Z. revised the manuscript.

Conflict of interest: The authors declare that they have no known competing financial interests or personal relationships that could have appeared to influence the work reported in this paper.

Funding

This work was supported in part by the USA National Institute of Health grants NHLBI R01 HL114120, HL131017, HL149137, UO1 HL134764.

Data availability

All data are incorporated into the article and its online supplementary material.

References

- 1. Lian X, Zhang J, Azarin SM, Zhu K, Hazeltine LB, Bao X, Hsiao C, Kamp TJ, Palecek SP. Directed cardiomyocyte differentiation from human pluripotent stem cells by modulating Wnt/beta-catenin signaling under fully defined conditions. Nat Protoc 2013;8:162–175. Wnt/beta-catenin signaling under fully defined conditions. Nat Protoc 2013;8:162-175.
- 2. Zhang S, Dutton JR, Su L, Zhang J, Ye L. The influence of a spatiotemporal 3D environment on endothelial cell differentiation of human induced pluripotent stem cells. *Biomaterials* 2014;**35**:3786–3793.
- 3. Yang L, Geng Z, Nickel T, Johnson C, Gao L, Dutton J, Hou C, Zhang J. Differentiation of o human induced-pluripotent stem cells into smooth-muscle cells: two novel protocols. PloS One 2016:11:e0147155.
- 4. Zhang J, Tao R, Campbell KF, Carvalho JL, Ruiz EC, Kim GC, Schmuck EG, Raval AN, da Rocha AM, Herron TJ, Jalife J, Thomson JA, Kamp TJ. Functional cardiac fibroblasts derived from human pluripotent stem cells via second heart field progenitors. *Nat Commun* 2019;**10**:
- 5. Chen IY, Matsa E, Wu JC. Induced pluripotent stem cells: at the heart of cardiovascular pre- $\overset{\omega}{\mathbb{Q}}$ cision medicine. Nat Rev Cardiol 2016;13:333-349.
- 6. Menasche P. Cell therapy trials for heart regeneration—lessons learned and future directions. Nat Rev Cardiol 2018;15:659-671.
- 7. Ye L, Chang YH, Xiong Q, Zhang P, Zhang L, Somasundaram P, Lepley M, Swingen C, Su L, 🥃 Wendel JS, Guo J, Jang A, Rosenbush D, Greder L, Dutton JR, Zhang J, Kamp TJ, Kaufman DS, 🔊 Ge Y, Zhang J. Cardiac repair in a porcine model of acute myocardial infarction with human 🔀 induced pluripotent stem cell-derived cardiovascular cells. Cell stem cell 2014; 15:750–761.
- 8. Wendel JS, Ye L, Zhang P, Tranquillo RT, Zhang JJ. Functional consequences of a tissueengineered myocardial patch for cardiac repair in a rat infarct model. Tissue Eng Part A 2014:20:1325-1335.
- 9. Tao Z, Loo S, Su L, Tan S, Tee G, Gan SU, Zhang J, Chen X, Ye L. Angiopoietin-1 enhanced myocyte mitosis, engraftment, and the reparability of hiPSC-CMs for treatment of myocardial infarction. Cardiovasc Res 2021;117:1578-1591.
- 10. Tan SH, Loo SJ, Gao Y, Tao ZH, Su LP, Wang CX, Zhang SL, Mu YH, Cui YH, Abdurrachim $D, Wang\ WH, Lalic\ J, Lim\ KC, Bu\ J, Tan\ RS, Lee\ TH, Zhang\ J, Ye\ L.\ Thymosin\ beta 4\ increases$ cardiac cell proliferation, cell engraftment, and the reparative potency of human inducedpluripotent stem cell-derived cardiomyocytes in a porcine model of acute myocardial infarction. Theranostics 2021;11:7879-7895.

 Takahashi K, Tanabe K, Ohnuki M, Narita M, Ichisaka T, Tomoda K, Yamanaka S. Induction of pluripotent stem cells from adult human fibroblasts by defined factors. *Cell* 2007;**131**: 861–872.

- Thomson JA, Itskovitz-Eldor J, Shapiro SS, Waknitz MA, Swiergiel JJ, Marshall VS, Jones JM. Embryonic stem cell lines derived from human blastocysts. Science 1998;282:1145–1147.
- Yu J, Hu K, Smuga-Otto K, Tian S, Stewart R, Slukvin II, Thomson JA. Human induced pluripotent stem cells free of vector and transgene sequences. Science 2009;324:797–801.
- 14. Gao L, Gregorich ZR, Zhu W, Mattapally S, Oduk Y, Lou X, Kannappan R, Borovjagin AV, Walcott GP, Pollard AE, Fast VG, Hu X, Lloyd SG, Ge Y, Zhang J. Large cardiac muscle patches engineered from human induced-pluripotent stem cell-derived cardiac cells improve recovery from myocardial infarction in swine. *Circulation* 2018;137:1712–1730.
- Feric NT, Radisic M. Maturing human pluripotent stem cell-derived cardiomyocytes in human engineered cardiac tissues. Adv Drug Deliv Rev 2016;96:110–134.
- Gabisonia K, Prosdocimo G, Aquaro GD, Carlucci L, Zentilin L, Secco I, Ali H, Braga L, Gorgodze N, Bernini F, Burchielli S, Collesi C, Zandona L, Sinagra G, Piacenti M, Zacchigna S, Bussani R, Recchia FA, Giacca M. MicroRNA therapy stimulates uncontrolled cardiac repair after myocardial infarction in pigs. Nature 2019;569:418–422.
- 17. Giacomelli E, Meraviglia V, Campostrini G, Cochrane A, Cao X, van Helden RWJ, Krotenberg Garcia A, Mircea M, Kostidis S, Davis RP, van Meer BJ, Jost CR, Koster AJ, Mei H, Miguez DG, Mulder AA, Ledesma-Terron M, Pompilio G, Sala L, Salvatori DCF, Slieker RC, Sommariva E, de Vries AAF, Giera M, Semrau S, Tertoolen LGJ, Orlova VV, Bellin M, Mummery CL. Human-iPSC-derived cardiac stromal cells enhance maturation in 3D cardiac microtissues and reveal non-cardiomyocyte contributions to heart disease. Cell Stem Cell 2020;26:862–879 e11.
- 18. Frangogiannis NG. Cardiac fibrosis. Cardiovasc Res 2021;117:1450–1488.
- Zhang J, Chu LF, Hou Z, Schwartz MP, Hacker T, Vickerman V, Swanson S, Leng N, Nguyen BK, Elwell A, Bolin J, Brown ME, Stewart R, Burlingham WJ, Murphy WL, Thomson JA. Functional characterization of human pluripotent stem cell-derived arterial endothelial cells. *Proc Natl Acad Sci U S A* 2017;**114**:E6072–E6078.
- Rosa S, Praca C, Pitrez PR, Gouveia PJ, Aranguren XL, Ricotti L, Ferreira LS. Functional characterization of iPSC-derived arterial- and venous-like endothelial cells. Sci Rep 2019;9:3826.
- Zhang L, Guo J, Zhang P, Xiong Q, Wu SC, Xia L, Roy SS, Tolar J, O'Connell TD, Kyba M, Liao K, Zhang J. Derivation and high engraftment of patient-specific cardiomyocyte sheet using induced pluripotent stem cells generated from adult cardiac fibroblast. Circ Heart Fail 2015;8:156–166.
- Tohyama S, Hattori F, Sano M, Hishiki T, Nagahata Y, Matsuura T, Hashimoto H, Suzuki T, Yamashita H, Satoh Y, Egashira T, Seki T, Muraoka N, Yamakawa H, Ohgino Y, Tanaka T, Yoichi M, Yuasa S, Murata M, Suematsu M, Fukuda K. Distinct metabolic flow enables large-scale purification of mouse and human pluripotent stem cell-derived cardiomyocytes. Cell Stem Cell 2013;12:127–137.
- 23. Su L, Kong X, Lim S, Loo S, Tan S, Poh K, Dutton J, Stewart C, Cook S, Su X, Ma J, Zhang J, Ye L. The prostaglandin H2 analog U-46619 improves the differentiation efficiency of human induced pluripotent stem cells into endothelial cells by activating both p38MAPK and ERK1/2 signaling pathways. Stem Cell Res Ther 2018;9:313.
- 24. Jackman CP, Carlson AL, Bursac N. Dynamic culture yields engineered myocardium with near-adult functional output. *Biomaterials* 2016;**111**:66–79.
- Lou X, Zhao M, Fan C, Fast VG, Valarmathi MT, Zhu W, Zhang J. N-cadherin overexpression enhances the reparative potency of human-induced pluripotent stem cell-derived cardiac myocytes in infarcted mouse hearts. *Cardiovasc Res* 2020;**116**:671–685.
- 26. Kahn-Krell A, Pretorius D, Guragain B, Lou X, Wei Y, Zhang J, Qiao A, Nakada Y, Kamp TJ, Ye L, Zhang J. A three-dimensional culture system for generating cardiac spheroids composed of cardiomyocytes, endothelial cells, smooth-muscle cells, and cardiac fibroblasts derived from human induced-pluripotent stem cells. Front Bioeng Biotechnol 2022;10:908848.
- Rosner B, Willett WC, Spiegelman D. Correction of logistic regression relative risk estimates and confidence intervals for systematic within-person measurement error. Stat Med 1989;8:1051–1069. Discussion 1071–1073.

- Rosner GL, Tsiatis AA. The impact that group sequential tests would have made on ECOG clinical trials. Stat Med 1989:8:505–516.
- Fan C, Tang Y, Zhao M, Lou X, Pretorius D, Menasche P, Zhu W, Zhang J. CHIR99021 and fibroblast growth factor 1 enhance the regenerative potency of human cardiac muscle patch after myocardial infarction in mice. *J Mol Cell Cardiol* 2020;**141**:1–10.
- Takagawa J, Zhang Y, Wong ML, Sievers RE, Kapasi NK, Wang Y, Yeghiazarians Y, Lee RJ, Grossman W, Springer ML. Myocardial infarct size measurement in the mouse chronic infarction model: comparison of area- and length-based approaches. J Appl Physiol (1985) 2007;102:2104–2111.
- Schilling J, Kelly DP. The PGC-1 cascade as a therapeutic target for heart failure. J Mol Cell Cardiol 2011;51:578–583.
- Huss JM, Kelly DP. Nuclear receptor signaling and cardiac energetics. Circ Res 2004;95: 568–578.
- 33. Miki K, Uenaka H, Saito A, Miyagawa S, Sakaguchi T, Higuchi T, Shimizu T, Okano T, Yamanaka S, Sawa Y. Bioengineered myocardium derived from induced pluripotent stem cells improves cardiac function and attenuates cardiac remodeling following chronic myocardial infarction in rats. Stem Cells Transl Med 2012;1:430–437.
- Wendel JS, Ye L, Tao R, Zhang J, Zhang J, Kamp TJ, Tranquillo RT. Functional effects of a tissue-engineered cardiac patch from human induced pluripotent stem cell-derived cardiomyocytes in a rat infarct model. Stem Cells Transl Med 2015;4:1324–1332.
- Huang S, Yang Y, Yang Q, Zhao Q, Ye X. Engineered circulatory scaffolds for building cardiac tissue. J Thorac Dis 2018;10:S2312–S2328.
- Yanamandala M, Zhu W, Garry DJ, Kamp TJ, Hare JM, Jun HW, Yoon YS, Bursac N, Prabhu SD, Dorn GW II, Bolli R, Kitsis RN, Zhang J. Overcoming the roadblocks to cardiac cell therapy using tissue engineering. J Am Coll Cardiol 2017;70:766–775.
- Huang NF, Serpooshan V, Morris VB, Sayed N, Pardon G, Abilez OJ, Nakayama KH, Pruitt BL, Wu SM, Yoon YS, Zhang J, Wu JC. Big bottlenecks in cardiovascular tissue engineering. Commun Biol 2018;1:199.
- 38. Pretorius D, Kahn-Krell AM, Lou X, Fast VG, Berry JL, Kamp TJ, Zhang J. Layer-by-layer fabrication of large and thick human cardiac muscle patch constructs with superior electrophysiological properties. *Front Cell Dev Biol* 2021;**9**:670504.
- Camelliti P, Borg TK, Kohl P. Structural and functional characterisation of cardiac fibroblasts. Cardiovasc Res 2005:65:40–51.
- Porter KE, Turner NA. Cardiac fibroblasts: at the heart of myocardial remodeling. *Pharmacol Ther* 2009;**123**:255–278.
- Radisic M, Park H, Martens TP, Salazar-Lazaro JE, Geng W, Wang Y, Langer R, Freed LE, Vunjak-Novakovic G. Pre-treatment of synthetic elastomeric scaffolds by cardiac fibroblasts improves engineered heart tissue. J Biomed Mater Res A 2008;86:713

 –724.
- Rupert CE, Kim TY, Choi BR, Coulombe KLK. Human cardiac fibroblast number and activation state modulate electromechanical function of hiPSC-cardiomyocytes in engineered myocardium. Stem Cells Int 2020;2020:9363809.
- Pretorius D, Kahn-Krell AM, LaBarge WC, Lou X, Kannappan R, Pollard AE, Fast VG, Berry JL, Eberhardt AW, Zhang J. Fabrication and characterization of a thick, viable bi-layered stem cell-derived surrogate for future myocardial tissue regeneration. *Biomed Mater* 2021;16: 035007
- Gao L, Wang L, Wei Y, Krishnamurthy P, Walcott GP, Menasche P, Zhang J. Exosomes secreted by hiPSC-derived cardiac cells improve recovery from myocardial infarction in swine. Sci Transl Med 2020;12:eaay1318.
- Hodgkinson CP, Bareja A, Gomez JA, Dzau VJ. Emerging concepts in paracrine mechanisms in regenerative cardiovascular medicine and biology. Circ Res 2016;118:95–107.
- Masumoto H, Matsuo T, Yamamizu K, Uosaki H, Narazaki G, Katayama S, Marui A, Shimizu T, Ikeda T, Okano T, Sakata R, Yamashita JK. Pluripotent stem cell-engineered cell sheets reassembled with defined cardiovascular populations ameliorate reduction in infarct heart function through cardiomyocyte-mediated neovascularization. Stem Cells 2012;30: 1196–1205.

Translational perspective

Heart transplantation surgery remains the only established treatment for end-stage heart disease, and the supply of donated hearts is far lower than the number of patients in need of treatment. Thus, the goal of cardiac tissue engineering is to replace the scarred region of an injured heart with functional cardiac muscle. The results presented in this report suggest that engineered human cardiac muscle patches may be more effective for the treatment of heart disease when they are constructed with cardiomyocytes, smooth muscle cells, endothelial cells, and cardiac fibroblasts than when the cardiac fibroblasts are omitted.